

Numerical simulation of dynamic Interactions of an arctic spar with drifting level ice

H.K. Jang*, H.Y. Kang and M.H. Kim

Department of Ocean Engineering, Texas A&M University, College Station, TX 77843, USA

(Received August 19, 2016, Revised October 13, 2016, Accepted October 20, 2016)

Abstract. This study aims to develop the numerical method to estimate level ice impact load and investigate the dynamic interaction between an arctic Spar with sloped surface and drifting level ice. When the level ice approaches the downward sloped structure, the interaction can be decomposed into three sequential phases: the breaking phase, when ice contacts the structure and is bent by bending moment; the rotating phase, when the broken ice is submerged and rotated underneath the structure; and the sliding phase, when the submerged broken ice becomes parallel to the sloping surface causing buoyancy-induced fictional forces. In each phase, the analytical formulas are constructed to account for the relevant physics and the results are compared to other existing methods or standards. The time-dependent ice load is coupled with hull-riser-mooring coupled dynamic analysis program. Then, the fully coupled program is applied to a moored arctic Spar with sloped surface with drifting level ice. The occurrence of dynamic resonance between ice load and spar motion causing large mooring tension is demonstrated.

Keywords: ice interaction; arctic spar; level ice; sloped surface; coupled dynamics; bending failure; breaking phase; rotating phase; sliding phase; ice-induced resonance; time domain analysis; platform motions; mooring forces

1. Introduction

Ice forces on structures have been investigated over the decades with growing interests in oil and gas exploration in arctic region where approximately 30% of the remaining oil and gas is reserved. Due to the increasing water depths for well development, moored floating platforms were proposed in spite of harsh environment conditions. International standard ISO 19906 provides the estimation of ice actions on offshore structures by presenting a couple of equations for various types of structures under different ice conditions. However, most information is limited to fixed structures rather than floating moored structures. Therefore, it is necessary to predict the ice forces acting on floating platforms reasonably and investigate the interaction between level ice and a floating structure.

In arctic region, the downward sloping structure near the mean water level is appealing since it causes the level ice to fail in bending so that the global ice load on the structure can be reduced. Nevel (1965) provided a formula for the vertical ice load by solving the semi-infinite plate on an

*Corresponding author, Ph.D. Student, E-mail: hj4345@tamu.edu

elastic foundation. Croasdale (1980) presented the two dimensional study about the level ice force on a sloping structure by assuming a beam on an elastic foundation. Ralston (1980) estimated the global level ice force on a conical structure by using plastic limit analysis. He derived the formula including the contributions from radial and circumferential cracks, foundation reaction, deforming region, ride-up component, and frictional dissipation. By utilizing the previous works, a number of researchers (e.g., Frederking and Timco 1985, Toyama and Yashima 1985, Aksnes 2010, Lu, Lubbad *et al.* 2014) further developed the formulas regarding the level-ice interactions with a sloping structure in three phases consisting of breaking, rotating, and sliding procedures.

In the current paper, we adopted the beam theory on an elastic foundation for the initial breaking phase. The given solution by Hetenyi (1946) for the semi-infinite ice-beam model subjected to the vertical and axial compression forces was considered with the geometric relation between ice and structure. Until the incoming ice fails in bending against the inclined structure, the governing equation of an elastic beam with the initial boundary condition is solved numerically and the ice tip deflection is calculated by the solution. Based on the given solution, the moment curve along the entire ice beam is checked whether it exceeds the allowable ice flexural strength. If so, the broken ice length is calculated, and the rotating ice phase is turned on. Since we assume that the intact level ice continuously approaches the structure with the constant speed, the broken ice would be gradually submerged and rotated downwards. During this process, the viscous drag forces and hydrostatic pressures are applied to the broken ice. Those are functions of the ice velocity and its position. Therefore, the dynamic governing equation of rotating ice including the ice inertia, restoring and exciting forces are solved every time step so that the instantaneous kinematics of the ice block can be obtained. Once the ice block becomes parallel to the sloped surface, the broken ice is sliding along the downward sloping structure, causing the frictional force. This friction force is basically induced by the buoyancy of the submerged ice. In this stage, it is assumed that after the specified depth, the ice block is detached and removed.

Based on the procedural time-dependent ice-load estimation, it is coupled with platform motions with mooring dynamics. The platform-mooring coupled dynamics program has been developed by the 3d author's research group during the past two decades (e.g., Kang and Kim 2012, Yang and Kim, 2010, 2011) with numerous verifications against experimental and field data. By adding the time-dependent ice-loading model on the time-domain simulation program, the dynamic interactions of the drifting level ice with moored arctic Spar is solved. As far as authors know, this kind of fully coupled ice-hull-mooring dynamic interaction has never been solved in the open literature.

2. Modelling of level ice forces interacting with a sloping structure

2.1 Ice breaking (or crushing) phase

According to ISO 19906, level ice can be defined as sea ice with un-deformed upper and lower surfaces. In order for offshore structures to resist the load by level ice, the inclined wall was proposed to induce the level ice failure against bending. If the ice floe is long and slender enough, and is subjected to the reaction forces at the edge, then the ice is to fail when the tensile stress reaches the ice flexural stress.

In this paper, a semi-infinite beam theory on elastic foundation is first employed. The beam equation on the elastic foundation (1) is subjected to the horizontal load, F_{BH} , and the vertical load,

F_{BV} is applied on the contact area between ice and a structure as a boundary condition (2).

$$EI \frac{d^4 v}{dx^4} + F_{BH} \frac{d^2 v}{dx^2} + \rho_w g B v = 0, \quad x > 0 \tag{1}$$

where E is the modulus of elasticity, I is the second moment of area of the ice-beam, ρ_w is the water density, g is the gravitational acceleration, B is the width of the ice-beam, v is the vertical deflection of ice, x is horizontal spatial variable. In order to obtain the analytical solutions of governing equation, boundary conditions are introduced. Since the ice is semi-infinite, the deflection and rotation are zeros at infinite x . On the other hand, the contact point is assumed to be a free end, where the moment is zero and vertical shear force is the applied force, F_{BV} .

$$\lim_{x \rightarrow -\infty} v(x) = 0, \quad \lim_{x \rightarrow -\infty} \frac{dv}{dx} = 0, \quad \frac{d^2 v(0)}{dx^2} = 0, \quad -EI \frac{d^3 v(0)}{dx^3} = -F_{BV} \tag{2}$$

The corresponding solutions given by Hetenyi (1946) are

$$v(x) = \frac{F_{BV}}{2EI \alpha (3\beta^2 - \alpha^2)} e^{-\beta x} (2\alpha\beta \cos \alpha x + (\beta^2 - \alpha^2) \sin \alpha x)$$

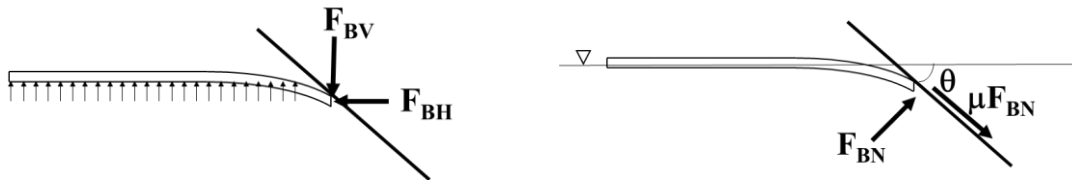
$$M(x) = -EI \frac{d^2 v(x)}{dx^2} = \frac{-2F_{BV} \lambda^2}{\alpha (3\beta^2 - \alpha^2)} e^{-\beta x} \sin \alpha x \tag{3}$$

and

$$\alpha = \sqrt{\lambda^2 + \frac{F_{BH}}{4EI}}, \quad \beta = \sqrt{\lambda^2 - \frac{F_{BH}}{4EI}}, \quad \lambda = \sqrt[4]{\frac{\rho_w g B}{4EI}}$$

One can find the force relation by manipulating the geometry and force balance at the contact point as shown in Fig. 1. The reaction forces can be decomposed into the normal and fictional forces at the contact point. The ISO standard also uses the vertical and horizontal forces relationship as follows

$$F_{BH} = \xi \cdot F_{BV}, \quad \xi = \frac{\sin \theta + \mu \cos \theta}{\cos \theta - \mu \sin \theta} \tag{4}$$



(a) Reaction forces on Ice (b) Applying force on a sloping structure

Fig. 1 Ice breaking procedure

When the drifting ice contacts with a sloping structure, the vertical deflection at a contact point can be calculated with the penetrated distance of level ice into the structure. It can be expressed as $v(0) = (v_{ice}t - X(t))\tan\theta$, where v_{ice} is the ice drift speed and X is the horizontal contact point coordinate.

Therefore, utilizing the all conditions and obtaining the analytical solutions, the forces acting on the structure can be computed at each time step. In addition, by checking the maximum moment along the level ice, the tensile stress from bending and axial loads can be calculated by Eq. (5).

$$\sigma_{ice} = \frac{6M}{Bh_i^2} - \frac{H}{Bh_i} \quad (5)$$

If the maximum stress reaches the flexural strength of ice, the ice is considered to be broken and the ice rotation module is initiated. Ice breaking length, L_B is calculated as the distance from the edge of the ice sheet to the point where the maximum stress occurs.

2.2 Ice rotating phase

Once the level ice is broken and the broken ice-block starts to be submerged, then the ice impact on a structure is computed from the ice rotation module immediately following the ice breaking module. This module runs until the ice block becomes parallel to the sloping surface. This process has been described in the papers of Liu, Lau *et al.* (2006) and Lu, Lubbad *et al.* (2014) stating that the ice block is subjected to the hydrodynamic force resulted from viscous drag as well as the static pressure from ventilation effects. The general process of rotating ice block is illustrated in Fig. 2.

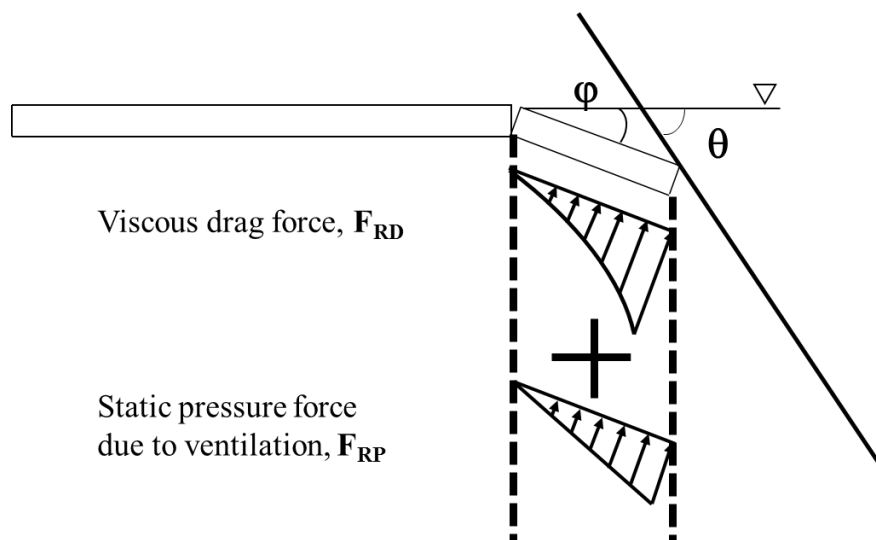


Fig. 2 Ice rotating procedure

2.2.1 Viscous drag force

During the ice rotation process, the ice block is assumed to be rotated around its rear edge and viscous drag force is applied to the ice block, which can be calculated by Eq. (6).

$$dF_{RD} = \frac{1}{2} \cdot \rho_w \cdot C_d \cdot B \cdot V_x^2 \cdot dx \quad (6)$$

By integrating over the breaking length, the viscous drag force acting on the ice block can be obtained with the velocity of the front edge of the ice block, V_{L_B} , in Eq. (7). From the paper by Kotras (1983), the drag coefficient, C_d , was selected to be 1.0.

$$F_{RD} = \frac{1}{6} \cdot \rho_w \cdot C_d \cdot B \cdot V_{L_B}^2 \cdot L_B \quad (7)$$

$$V_{L_B} = L_B \cdot \dot{\varphi}$$

2.2.2 Static pressure due to ventilation

Static pressure due to ventilation is estimated based on the theories by Lindstrom (1990). Ventilation means that the water on the broken ice top is free from flooding. This factor relies on different conditions such as the size and shape of broken ice, relative velocity and so on. In this paper, the static pressure is assumed to be applied on the beam linearly underneath the rotating ice block and it is factored by the coefficient, C_p . The static pressure force is

$$F_{RP} = C_p \cdot B \cdot L_B \cdot \rho_w \cdot g \cdot H_s \quad (8)$$

where $B \cdot L_B$ is the area of the ice block, H_s is the depth of the whole turning ice block, C_p is a coefficient determined by experimental or measured field data. In this simulation, the coefficient, C_p was selected to be zero, because the structure is a mobile floating type, and the level ice moves slowly, so ventilation is not likely to happen.

2.2.3 Rotating ice dynamic equation

For simplicity, we assume the breaking point as a hinge, and formulate the moment equilibrium for the rotating ice with reaction forces, F_{RH} and F_{RD} . Since the static pressure and viscous drag forces are proportional to the first and third power of the breaking length, the moment arm can be obtained as 2/3 and 4/5 of the breaking length, respectively. As the broken ice is considered as rigid, the angle between the broken ice and mean water level can be obtained as well as its kinematics by the geometry relations.

$$\begin{aligned} \sum M_{hinge} : & (1 + C_{added}) \left(\frac{1}{12} \rho_i B L_B h_i L_B^2 + \frac{1}{4} \rho_i B L_B h_i L_B^2 \right) \ddot{\varphi} + \frac{1}{2} L_B (\rho_w - \rho_i) B L_B h_i g \cos \varphi \\ & = L_B (F_{RV} \cos \varphi + F_{RH} \sin \varphi) - L_B \left(\frac{2}{3} F_{RP} + \frac{4}{5} F_{RD} \right) \end{aligned} \quad (9)$$

The added mass coefficient for the rotating motion of the plate around one edge was calculated based on the 3D panel-based radiation calculation using potential theory. Through the pre-processing, the added moment of inertia was obtained in the discretised length and interpolated for the corresponding the breaking length. With the obtained reaction forces, the moment

distribution along the broken ice length is checked for the secondary ice breaking and whether it exceeds the maximum moment corresponding to the ice flexural strength. After the second breaking, the broken ice is considered to resist the bending and be able to rotate as a rigid piece.

2.3 Ice sliding phase

In the ice sliding phase, the frictional force is caused by the ice buoyancy forces and ice sliding. The buoyancy force is

$$F_{SS} = (\rho_w - \rho_i) \cdot g \cdot B \cdot h_i \cdot \frac{Z}{\sin \theta} \quad (10)$$

where Z is the water depth of sliding ice. Moored structures in arctic region more likely have a sloped wall, and it would push ice sideways. Therefore, the limited amount of ice would slide under the structure up to the limited depth Z . Barker and Sayed (2012), Barker, Sudom *et al.* (2015) emphasized the importance of Z , stating that the ride-up height influenced the magnitude of global ice action. In Mayne and Brown (2000), they observed the rubble pile heights of Confederation Bridge and found that it depended on the ice thickness as a power law form as in Eq. (11). Even though a slope was upward, we directly adopted the equation in this simulation.

$$Z = 7.6h_{ice}^{0.64} \quad (11)$$

Manipulating the force relationship as shown in Fig. 3, the horizontal and vertical ice forces acting on the structure can be calculated as follows

- Reaction forces

$$\begin{cases} F_{SN} = F_{SS} \cos \theta \\ F_{ST} = \mu F_{SN} \end{cases} \quad (12)$$

- Forces applying to the structure

$$\begin{cases} F_{SH} = F_{ST} \cos \theta + F_{SN} \sin \theta \\ \quad = (\rho_w - \rho_i) \cdot g \cdot B \cdot h_i \cdot Z \cdot \cot \theta \cdot (\mu \cos \theta + \sin \theta) \\ \\ F_{SV} = F_{SN} \cos \theta - F_{ST} \sin \theta \\ \quad = (\rho_w - \rho_i) \cdot g \cdot B \cdot h_i \cdot \frac{Z}{\sin \theta} \cdot (\cos^2 \theta - \mu \cos \theta \sin \theta) \end{cases} \quad (13)$$

2.4 Coupled dynamic simulation considering ice-structure interaction

The current development has been achieved by extending the existing hull-riser-mooring coupled dynamic program, CHARM3D, which has been developed by the research group of the 3rd author during the past 20 years. Authors have successfully extended the program to analyze the ice-structure interaction for floating moored structures in time domain, including hydrodynamic effects. The governing equation for the floating structure is

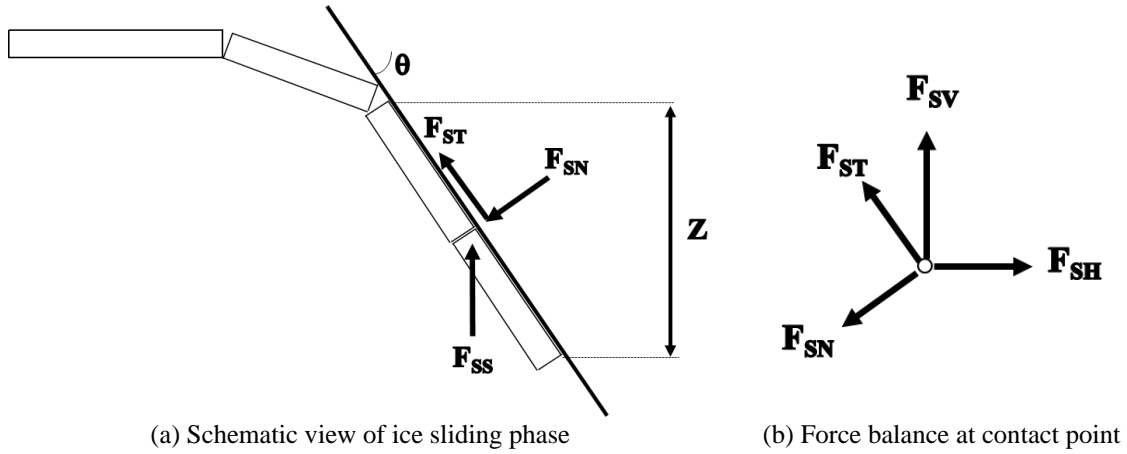


Fig. 3 Ice sliding procedure

$$(M + M_{Add}(\infty))\ddot{x}(t) + (K_{hydro})x(t) = F_{wave} + F_{convolution} + F_{drag} + F_{mooring} + F_{Brk} + F_{Rot} + F_{Sld} \tag{14}$$

where M is the mass of a structure, M_{add} is the added mass, K_{hydro} is the hydrostatic coefficients, F_{wave} is the wave exciting force, $F_{convolution}$ is the radiation-damping force, F_{drag} is the nonlinear drag force, $F_{mooring}$ is the mooring tension force, F_{Brk} , F_{Rot} , and F_{Sld} are ice induced forces by breaking, rotating, and sliding respectively.

Based on the original CHARM3D program, the ice load calculation module was added to calculate the external ice forces in time domain. Fig. 4 shows the flow chart of the CHARM3D ice module. With multiple input information, this simulator can additionally output the results of ice load time-series for each phase, ice breaking length, the broken ice kinematics and so on.

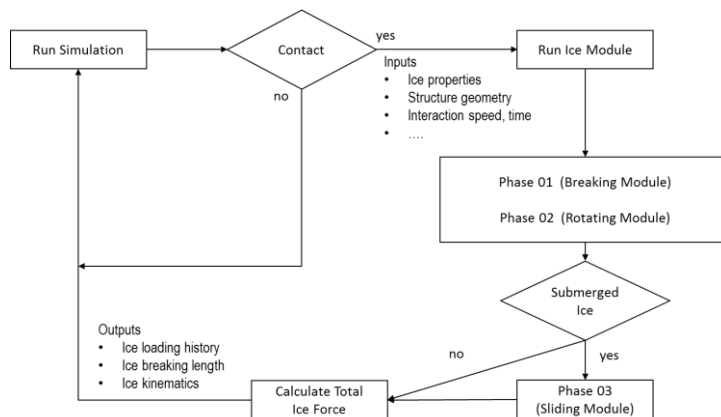


Fig. 4 Flow chart for ice interaction

3. Numerical model description

For a case study, we designed the generic model of a Spar-type floating structure with 14 mooring lines. In order to minimize the 3D-effect, the structure was modelled with the square cross-section as well as a flat inclined wall. The downward inclined angle was 45 degrees so that the ice may be failed by bending moment. Since the structure is floating-type, the inclined wall angle with respect to the waterline can vary in time with pitch motions, affecting the calculation of the ice load.

The free-decay test was conducted to identify the entire system. The hydrodynamic coefficients including added mass and radiation damping were calculated from the 3D panel-based radiation program. A drag coefficient of 1.5 was selected for the square type column. The natural frequencies of 6 degrees of freedom are tabulated in Table 3.

Table 1 Structure properties

Parameter	unit	Value
Displacement	MT	2129860
Width at MWL	m	40
Draft	m	182
Slope angle at MWL	deg.	40
Number of mooring lines	ea	14
COG below MWL	m	102.4
COB below MWL	m	99.5
Roll, Pitch Radius Gyration	m	122.6
Yaw Radius Gyration	m	8.7
Water Depth	m	914.4

Table 2 Mooring properties

Type	Unit	Value
No. Mooring Lines	ea	14
Chain	Dry/Wet weight	370.93 / 322.71
	Axial Stiffness	1.328E+06
	Added Nass	48.22
Wire	Dry/Wet weight	99.10 / 19.79
	Axial Stiffness	1.628E+06
	Added Nass	19.79
Unstretched Length	m	1402.98

Table 3 Arctic Spar natural frequencies

	Period (sec)	Frequency (rad/sec)
Surge	272.3	0.0231
Heave	24.7	0.2513
Pitch	39.0	0.1571

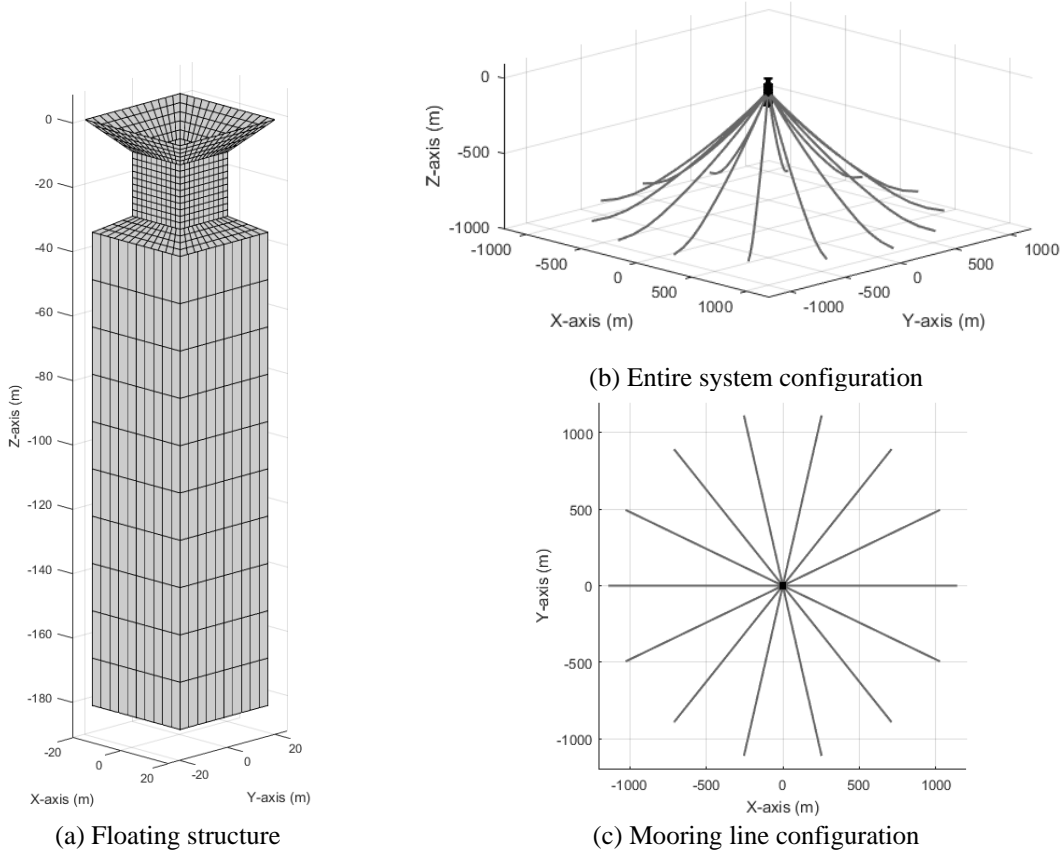


Fig. 5 Moored floating structure system model

The ice properties for the calculation of impact loading are tabulated in Table 4. According to ISO 19906, the range of the sea ice density is from 720 kg/m³ to 920 kg/m³ and above the waterline, the density ranges from 840 kg/m³ to 910kg/m³ for first-year ice. Therefore, the density of 900 kg/m³ was selected for the level ice in this simulation. In addition, the downward breaking flexural strength for winter has typical values of 0.3 MPa to 0.5 MPa, whereas 0.2 MPa is typical for warmer conditions. The elastic modulus of 4 GPa was selected considering that those of design ice actions in natural ice sheets range between 2 GPa and 6 GPa.

Table 4 Level ice properties

Parameter	Value	unit
Flexural strength, σ_f	500	kPa
Ice thickness, h_i	2	m
Young's modulus, E	4	GPa
Friction coefficient, μ	0.1	-
Ice density, ρ_i	900	Kg/m ³

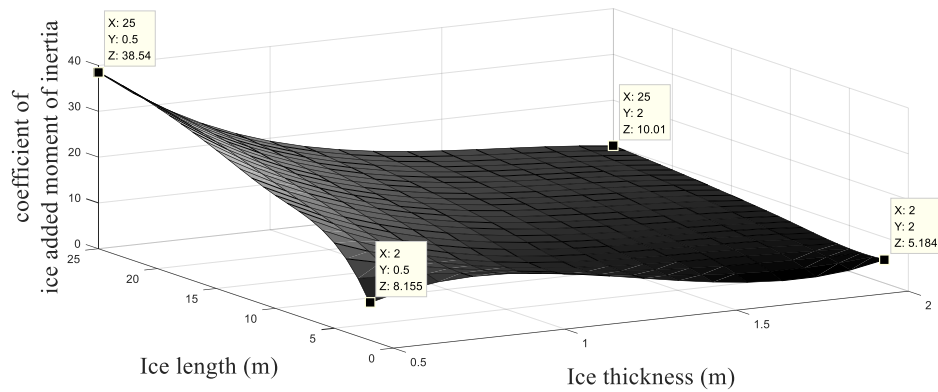


Fig. 6 Ice added moment of inertia coefficient

As a pre-processing, the ice added moment of inertia coefficient was calculated with potential theory. The rectangular shape with the width of 40m was considered. In the simulation, the coefficients for various ice thicknesses and breaking lengths were obtained. The interpolated values are shown in Fig. 6.

4. Numerical simulation results and discussions

4.1 Total Ice load estimation

The total ice load in the 3 hour long simulation shows repeating pattern of load signals with certain period. This period is determined by the breaking length and the drifting speed of level ice as well as the interaction with the structure. With the given ice properties, level ice is very stiff, and thus the level ice is broken in a very short time despite small tip deflection. The breaking force is a function of the sloped angle of the structure, which slightly varies in time due to small pitch motions. After the breaking, the broken ice is rotated downward along the inclined structure surface. In the rotating phase, the simulation shows a peak at first and its magnitude monotonically decreases after that until we have another peak by the initial contact (breaking phase) of the second broken ice sheet. Through the results, it was found that the second breaking occurred right after the first breaking due to the large reaction forces at contact point. Once the ice was broken into two parts, the broken ice was rotated sequentially until each one became parallel to the structure. The rotating ice force in surge direction decreases with increasing angle in time. The reduction of angular velocity also contributes to the reduction of drag-induced surge force. At the time when the broken ice becomes parallel with the surface, the buoyancy-induced contact force becomes maximum which corresponds to the peak of sliding force.

For comparison, two other methods were also selected. Croasdale (1980) initially considered two dimensional upward-slope fixed structure for level ice impact and he used the beam equation on elastic foundation for breaking force. He added the force contribution to push up the broken ice. Croasdale (1994) has further developed the equations including rubble effects. For the

downward-slope floating structure, we assume that the rubble effects are negligible, as moored platform is moveable, which was also seen in Bruun, Husvik *et al.* (2009). By this fact, we considered only two components of breaking and ride-down force. By replacing the ice density to the difference of water and ice densities, the level ice force for a downward sloping structure can be calculated as follows

$$F_{horizontal} = 0.68B\sigma_f \sqrt[4]{\frac{\rho_w g h_i^5}{E} \frac{\sin \theta + \mu \cos \theta}{\cos \theta - \mu \sin \theta}} + BZ h_i (\rho_w - \rho_{ice}) g \left(\frac{(\sin \theta + \mu \cos \theta)^2}{\cos \theta - \mu \sin \theta} + \frac{\sin \theta + \mu \cos \theta}{\tan \theta} \right) \quad (14)$$

Ralston (1980) also studied the level ice impact acting on a conical structure. He derived the formula consisting of contributions from radial, circumferential cracks, foundation reaction, deforming region, ride-up component and frictional dissipation. The detailed theory and equations are given in Ralston (1980). In the comparison, the formulas given by the ISO standard were used with the Tresca yielding condition.

Since these two methods do not account for the ice-velocity effects, the simulated results were calculated with the ice drift speed of 0.5 m/s for comparison. In all cases, the ice load increased with the increasing ice thickness. In this example, the simulation results are closer to those of Croasdale method.

According to the simulation results, the breaking and sliding forces increased linearly with the ice thickness. It was because these forces were proportional to the ice stiffness and volume. The rotating ice force also increased as the ice thickness became larger. The thicker level ice resulted in longer ice breaking length which caused larger fluid interaction forces. In this simulation, the ventilation effect was neglected by assuming that the water would be filled back right after the ice rotation. It is also assumed that the width of the level ice pushing the platform is the same as the column width, which may be the case when cracks happen at both edges of the square column.

Table 5 Global ice load comparison

Ice Thickness (m)	0.5	0.8	1.0	1.3	1.5	1.8	2.0
Ralston (MN)	0.666	1.487	2.184	3.444	4.421	5.506	7.328
Croasdale (MN)	0.485	0.948	1.306	1.910	2.352	2.823	3.582
Simulation (MN)	0.475	0.938	1.304	1.927	2.400	3.139	3.689

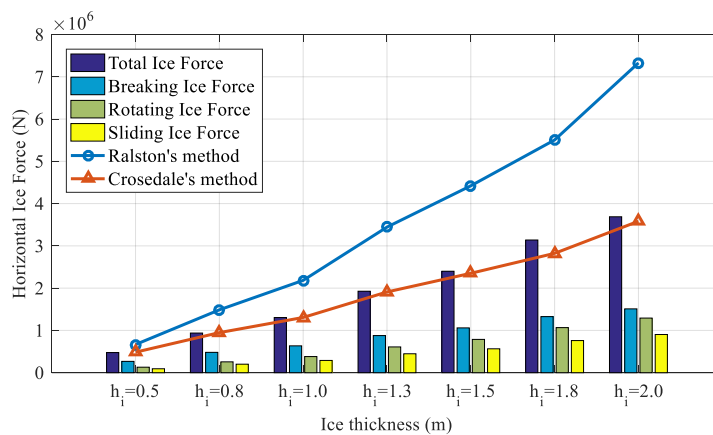
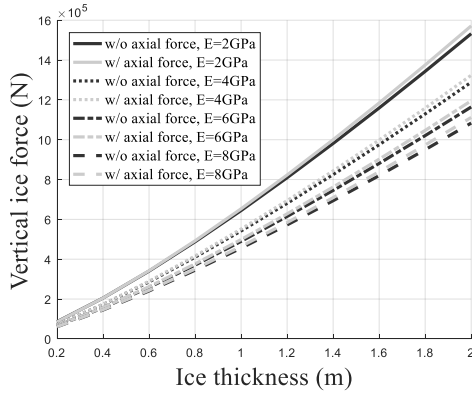
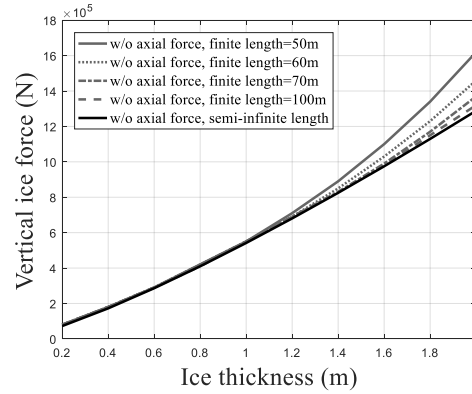


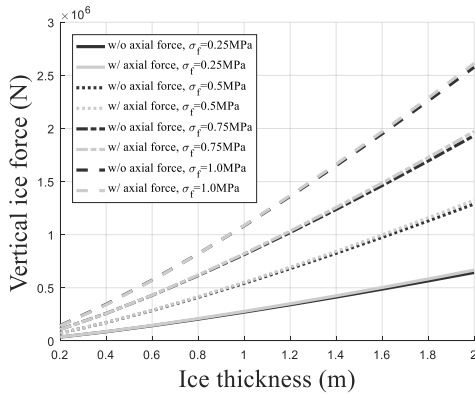
Fig. 8 Ice force contribution of each phase with varying ice thickness (Maximum values)



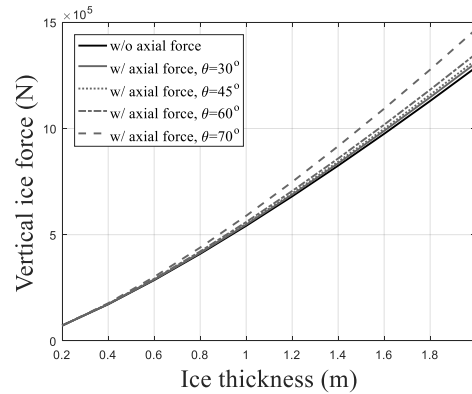
(a) Vertical ice load with thickness by varying Elastic Modulus



(b) Vertical ice load with thickness by varying finite level ice length



(c) Vertical ice load with thickness by varying flexural strength



(d) Vertical ice load with thickness by varying inclined angle

Fig. 9 Effects of variables on a beam theory

4.2 Discussion about breaking phase

In this simulation, the beam equation with axial and vertical loads on an elastic foundation was used (e.g., Hetenyi 1946). For comparison, various cases under different conditions were investigated; semi-infinite beam equation subjected to the vertical load only, semi-infinite beam equation subjected to both vertical and axial loads, and finite beam equation subjected to the vertical load only. Fig. 9 shows the simulation results. As the elastic modulus is increased from 2GPa to 8GPa with an increment of ice thickness from 0.2 m to 2.0 m, having the axial compression component gives slightly higher breaking force. However, consideration of the finite length of level ice does not significantly influence the ice forces as long as the length of level ice is over 100 m as in this case.

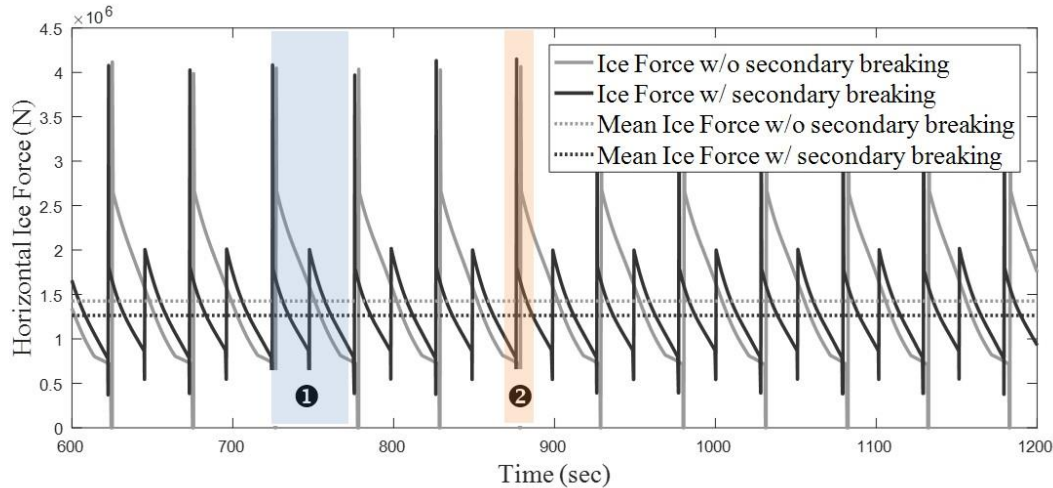


Fig. 10 Total ice force behavior with and without second breaking ($h_{ice}=2$ m, $v_{ice}=0.5$ m/s)

4.3 Second breaking scenario in rotating phase

In the model test conducted by Matsuishi and Ettema (1985), they observed that the ice interacting with the moored conical structure experienced the secondary ice breaking. During the rotating phase in the current simulation model, the possibility of secondary ice breaking was checked through observing bending moment distribution and local stress along the broken ice. The secondary breaking actually happened immediately after the first breaking (❷). As shown in Fig. 10, the comparison of numerical results between the cases w/ and w/o secondary breaking was made. Without secondary breaking, the ice loads monotonically decrease with time within one period. When secondary breaking occurs, there exist two peaks in one period (❶). Once the intact ice was broken, the first breaking length of 25 m was calculated. It was about 12.7 times the ice thickness. The secondary breaking immediately followed the first breaking. The reason for the second peak after the half period in this case is due to the initial impact (breaking phase) of the second portion following the frontal part. Since it is assumed that the attachment length of the sliding ice sheets is fixed in the model, the buoyancy induced sliding force caused by the displaced volume of surface-contacting ice sheets starts to decrease with the rotation of upper ice sheet. In the present modelling of the rotating phase, we have neglected the ventilation effects since the upper surface of ice is to be immediately flooded by sea water. If ventilation effects are taken into consideration in the beginning of rotation, the relevant force is generally large and the pattern of ice loading can be quite different.

In the field observation, the eventual ice breaking length varied in the range of approximately 3 to 10 times the ice thickness (ISO 19906, 2010). In the simulation, the first ice breaking length, which is the analytical solution by a beam equation, tended to be larger than the field observation. By applying the secondary ice breaking procedure, the breaking length was in the range suggested by ISO 19906.

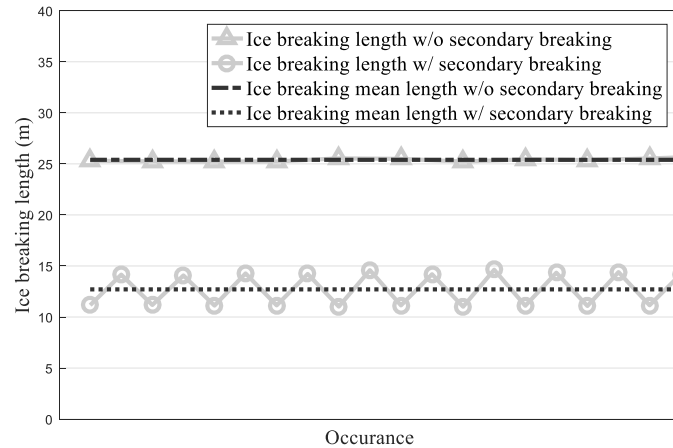
Fig. 11 Breaking Length Comparison, ($h_i=2$ m)

Table 6 Average value of breaking length and ratio when including secondary breaking

Ice Thickness (m)	0.5	0.8	1.0	1.3	1.5	1.8	2.0
Mean breaking length (m)	4.47	6.36	7.53	9.17	10.22	11.72	12.69
Ratio	8.94	7.95	7.53	7.06	6.81	6.90	6.34

4.4 Platform motions

Since the present level ice load on a sloping structure is relatively smaller than the forces induced by the ridge ice or iceberg, the platform responses generally show small offset and oscillating motions. In the simulation, the negative relative velocity of the ice with respect to the platform implies that the sliding broken ices are detached from the structure and drifted away from the structure. As a result, zero force is applied on a structure from that portion. For the rotating broken ice, the detachment of the ice block can be found by the geometrical consideration in each time step. Therefore, at very low ice drift speed, detachment occurs when the platform moves faster than the level ice (⊙). For this reason, the maximum total ice force at the low drift speed is smaller than other cases. When the level ice moves fast enough so that ice is not detached from the structure, then the structure exhibits small oscillating motions at its natural frequency. When the ice load frequency is close to the natural frequency of the platform, the response of the platform becomes amplified due to resonance. At the ice drift speed of 0.05 m/s and 0.1 m/s, the ice load energy is concentrated at the region close to the platform surge natural frequency of 0.02 rad/sec. The surge motion is strongly coupled with pitch motion, whose natural frequency is at 0.16 rad/sec, when ice drift speed is 0.3 m/s.

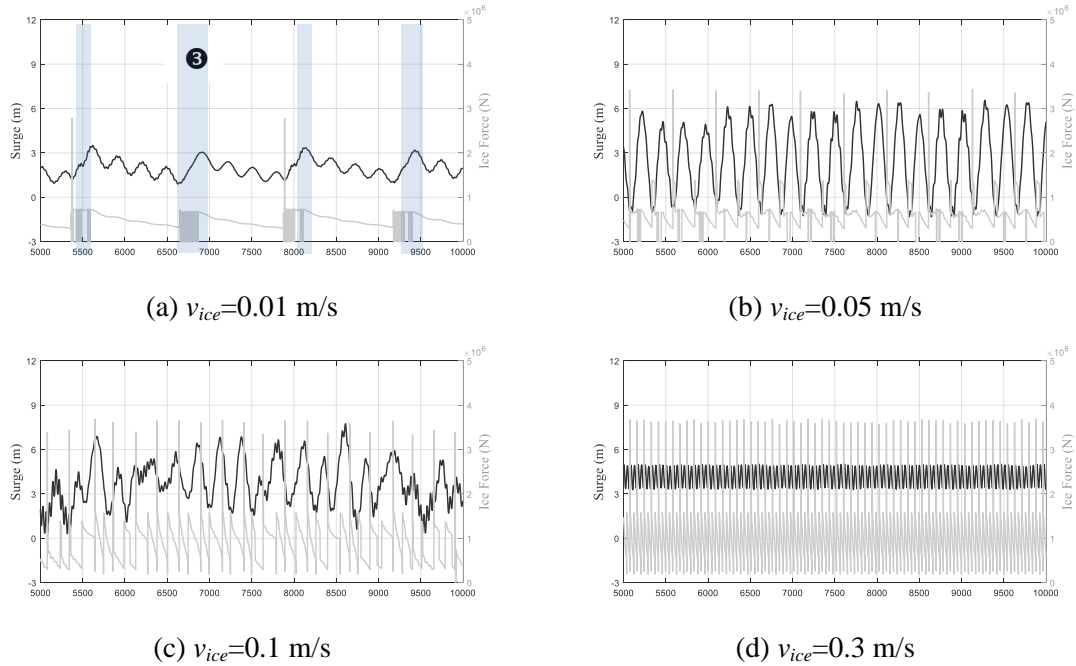


Fig. 12 Time series of platform surge motion (dark) and ice load (light) with varying drift velocity

 Table 7 Statistics of platform surge motions with varying ice drift velocity ($h_{ice} = 2$ m)

Ice drift velocity	0.01	0.05	0.1	0.3	0.5	0.8	1
Max.	3.497	6.556	7.750	5.022	4.419	4.450	4.470
Min.	0.895	-1.368	0.306	3.280	4.044	4.054	4.149
Mean.	1.969	2.455	3.727	4.160	4.229	4.250	4.312
Std.	0.576	2.407	1.518	0.550	0.075	0.079	0.067

4.5 Mooring dynamics and statistics

The mooring forces are generally proportional to the platform surge motions. Therefore, its pattern and statistical results are similar to those of platform surge motions. At low drift speeds about 0.1m/s, the mooring system experiences the largest forces, while its mean value is slightly dropped due to the interval of detachment between ice and platform.

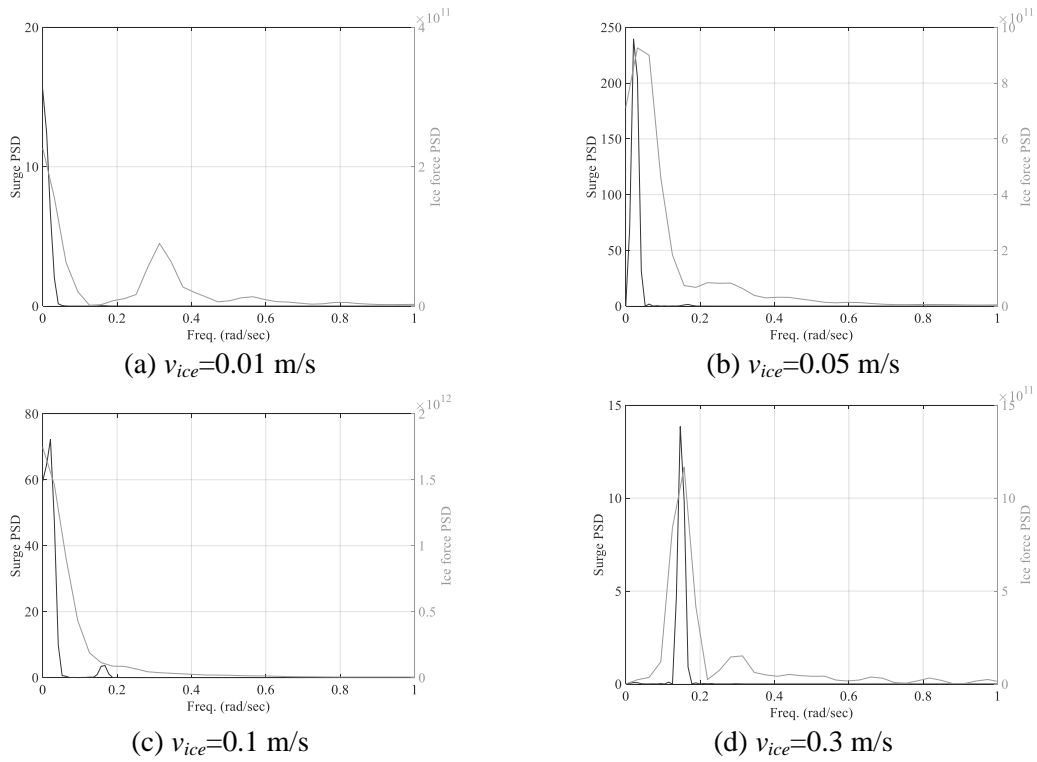


Fig. 13 Spectra of platform surge motion (dark) and ice load (light) with varying drift velocity

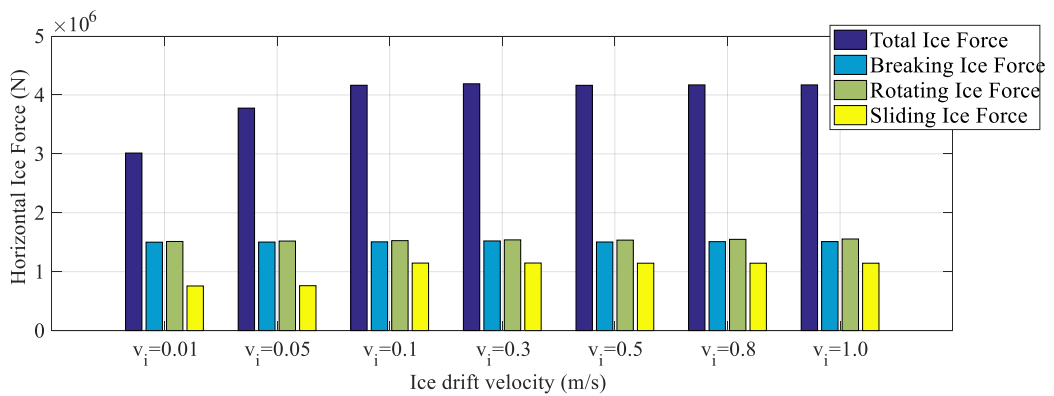


Fig. 14 Ice force contribution of each phase with varying ice drift velocity (Maximum values)

5. Conclusions

A time-domain numerical simulation procedure for predicting level ice load acting on the sloped floating structure and the interaction between them has been investigated in this study. To achieve this, three interacting phases were considered with analytical and theoretical formulas considering the relevant physics. In the breaking phase, the level ice was assumed to be a semi-infinite beam on an elastic foundation, and the corresponding solutions were adopted to calculate the breaking load and length. During the rotating phase, the fluid inertia and viscous forces are involved and by constructing the moment distribution curve, the secondary breaking was also simulated. After the broken ice became parallel to the structure, the buoyant and frictional forces were obtained in the sliding phase. Through the numerical simulations, several remarks can be made.

- Generally, the global ice loads were repeated with certain period, which was determined by the ice velocity and breaking length. The ice loads induced by bending failure were relatively smaller than other typical design loads by ice ridge, iceberg, or harsh wave conditions.
- The simulated maximum global forces were compared with the Ralston and Croseale methods, and they were in reasonable agreement.
- Considering the presence of axial force, slightly higher breaking force was obtained than that without it. The consideration of finite level ice length did not show big differences in breaking loads as long as the length was larger than 100 m.
- The secondary breaking occurred immediately following the first breaking, and it gave the similar breaking length with observed data, which was in a range of 3 to 10 times ice thickness.
- The numerical simulation demonstrated the possibility of resonance between ice loads and platform motions.
- Platform surge motions at low ice-drift speeds were larger as a result of the resonance between ice loads and platform motions. At high drift speeds, the ice load frequency is far from platform surge natural frequency and the resulting motions were small.
- The pattern of mooring tensions was similar to that of surge motions.

In the next study, the presence of winds, waves, and currents will be added to the present system.

Acknowledgments

The present research was financially supported by US DOE (Department of Energy) RPSEA Program.

References

- Aksnes, V. (2010), "A simplified interaction model for moored ships in level ice", *Cold Reg. Sci. Technol.*, **63**(1), 29-39.
- Barker, A. and Sayed, M. (2012), "Upward-or downward-breaking cones in ice: which one should you use", *Proceedings of the 15th International Conference on Cold Regions Engineering*, Canadian Society of Civil Engineers (CSCE), Quebec, Canada.
- Barker, A., Sudom, D. and Sayed, M. (2015), "Conical Structures in Ice: Ride-Up, Radius and Results",

- OTC Arctic Technology Conference.*
- Bruun, P.K., Husvik, J., Le Guennec, S. and Hellmann, J.H. (2009), "Ice model test of an Arctic SPAR", *Proceedings of the 20th International Conference on Port and Ocean Engineering Under Arctic Conditions.*
- Croasdale, K.R. (1980), Ice forces on fixed rigid structures, Special report 80-26, U.S. Army Cold Regions Research and Engineering Laboratory, Hanover
- Croasdale, K.R., Cammaert, A.B. and Metge, M. (1994), "A method for the calculation of sheet ice loads on sloping structures", *IAHR Ice Symposium*, Trondheim, Norway.
- Frederking, R.M.W. and Timco, G.W. (1985), "Quantitative analysis of ice sheet failure against an inclined plane", *J. Energ. Resour. Technol.*, **107**(3), 381-387.
- Hetényi, M. (1946), *Beams On Elastic Foundation;: Theory With Applications In The Fields Of Civil And Mechanical Engineery*, University of Michigan press.
- ISO (2010), *ISO 19906:2010 Petroleum and natural gas industries – Arctic offshore structures.*
- Kang, H.Y. and Kim, M.H. (2012), "Hydrodynamic interactions and coupled dynamics between a container ship and multiple mobile harbors", *Ocean Syst. Eng.*, **2**(3), 217-228.
- Kotras, T.V. (1983), "Predicting ship performance in level ice", *SNAME Trans*, **91**, 329-349.
- Lindstrom, C.A. (1990), "Numerical estimation of ice forces acting on inclined structures and ships in level ice", *Offshore Technology Conference.*
- Liu, J., Lau, M. and Williams, F.M. (2006), "Mathematical modeling of ice-hull interaction for ship maneuvering in ice simulations", *Proceedings of the 7th International Conference and Exhibition on Performance of Ships and Structures in Ice*, Banff, Alberta, July
- Lu, W., Lubbad, R., Høyland, K. and Løset, S. (2014), "Physical model and theoretical model study of level ice and wide sloping structure interactions", *Cold Reg. Sci. Technol.*, **101**, 40-72.
- Matsuiishi, M. and Ettema, R. (1985), *The Dynamic Behavior Of A Floating, Cable-Moored Platform Continuously Impacted By Ice Floes*: Iowa Institute of Hydraulic Research, the University of Iowa.
- Mayne, D.C. and Brown, T.G. (2000), "Rubble pile observations", *Proceedings of the 10th International Offshore and Polar Engineering Conference.*
- Nevel, D.E. (1965), "A semi-infinite plate on an elastic foundation", DTIC Document.
- Ralston, T.D. (1980), *Plastic Limit Analysis Of Sheet Ice Loads On Conical Structures.-Physics And Mechanics Of Ice*, 289-308. Springer.
- Toyama, Y. and Yashima, N. (1985), "Dynamic response of moored conical structures to a moving ice sheet", *Proceedings of the 8th International Conference on Port and Ocean Engineering under Arctic Conditions.*
- Wille, S.F., Kuiper, G.L. and Metrikine, A.V. (2011), "On the dynamic interaction between drifting level ice and moored downward conical structures: a critical assessment of the applicability of a beam model for the ice", *Proceedings of the 30th International Conference on Ocean, Offshore and Arctic Engineering.*
- Yang, C.K. and Kim, M.H. (2010), "Transient effects of tendon disconnection of a TLP by hull–tendon–riser coupled dynamic analysis", *Ocean Eng.*, **37**(8), 667-677.
- Yang, C.K. and Kim, M.H. (2011), "The structural safety assessment of a tie-down system on a tension leg platform during hurricane events", *Ocean Syst. Eng.*, **1** (4), 263-283.